

# A Perfectly Matched Layer for the Absorption of Electromagnetic Waves

JEAN-PIERRE BERENGER

*Centre d'Analyse de Défense, 16 bis, Avenue Prieur de la Côte d'Or, 94114 Arcueil, France*

Received July 2, 1993

---

A new technique of free-space simulation has been developed for solving unbounded electromagnetic problems with the finite-difference time-domain method. Referred to as PML, the new technique is based on the use of an absorbing layer especially designed to absorb without reflection the electromagnetic waves. The first part of the paper presents the theory of the PML technique. The second part is devoted to numerical experiments and to numerical comparisons with the previously used techniques of free-space simulation. These comparisons show that the PML technique works better than the others in all cases; using it allows us to obtain a higher accuracy in some problems and a release of computational requirements in some others. © 1994 Academic Press, Inc.

---

## 1. INTRODUCTION

Since the initial work of K. S. Yee [1], the finite-difference time-domain technique has been widely used in electromagnetic computations. One of the inconveniences of this technique lies in the fact that the Maxwell equations have to be solved in a discretized domain whose sizes need to be restrained. Nevertheless, open problems involving theoretically boundless space extension can be solved when applying special conditions on the boundaries of the computational domain, in order to absorb the outgoing waves. Such a need of free-space simulation happens in many problems and especially in wave-structure interactions.

To absorb the outgoing waves, various techniques have been used in computer codes. The first one was the "radiating boundary" [2, 3] which seems to be left unused now. Another one was the matched layer [4–6] which consisted of surrounding the computational domain with an absorbing medium whose impedance matches that of free-space. A third technique appeared with the one-way approximation of the wave equation initially exhibited for acoustic waves by Engquist and Majda [7]. Then applied in the electromagnetic field [8] this technique has been the purpose of many works [9, 10] and seems to be the most used today. However, none of the free-space simulation techniques is faultless; a wave is absorbed without reflection in particular cases only, for instance, if it is plane

and propagates perpendicularly to the boundary. These imperfections forbid treatment of some problems and impose constraints on others, as the well-known need of setting boundaries sufficiently far from the scatterer when solving interaction problems.

In this paper, we describe a new technique of free-space simulation. As in [4–6] this technique is based on the use of an absorbing layer, but the matched medium of [4–6] is now replaced by a new matched medium that we have especially designed to absorb without reflection the electromagnetic waves. With the new medium the theoretical reflection factor of a plane wave striking a vacuum-layer interface is null at any frequency and at any incidence angle, contrary to the [4–6] medium with which such a factor is null at normal incidence only. So, the layer surrounding the computational domain can theoretically absorb without reflection any kind of wave travelling towards boundaries, and it can be regarded as a perfectly matched layer. Further, we will refer to the new medium as the PML medium and to the new technique of free-space simulation as the PML technique.

The first part of the paper describes the PML technique for two-dimensional problems. The PML medium is defined, its theoretical reflectionless properties at a vacuum-layer interface are proved, and then the implementation of the PML technique in a finite-difference computational domain is addressed. The second part of the paper is devoted to numerical experiments in order to evaluate how the theoretical properties of the PML technique are preserved in practical computations. Various numerical tests are addressed: reflection of a plane wave at a vacuum-layer interface, absorption of a pulse on boundaries of a computational domain, wave-structure interaction problems, and radiation of a slot in free-space. In each case, the results computed with the PML technique are compared to those computed using the matched layer [4–6] and the one-way wave equation both in its initial form [7, 8] and in the Higdon operator form [9]. These comparisons show that the PML technique brings a real enhancement of computed results in all cases.

## 2. THEORY OF THE PERFECTLY MATCHED LAYER

### 2.1. Definition of the PML Medium

In this paper, we will set the equations of a PML medium for two-dimensional problems, first in the TE (transverse electric) case. In Cartesian coordinates let us consider a problem that is without variation along  $z$ , with the electric field lying in the  $(x, y)$  plane (Fig. 1). The electromagnetic field involves three components only,  $E_x$ ,  $E_y$ ,  $H_z$ , and the Maxwell equations reduce to a set of three equations. In the most general case, which is a medium with an electric conductivity  $\sigma$  and a magnetic conductivity  $\sigma^*$ , these equations can be written as

$$\epsilon_0 \frac{\partial E_x}{\partial t} + \sigma E_x = \frac{\partial H_z}{\partial y} \quad (1.a)$$

$$\epsilon_0 \frac{\partial E_y}{\partial t} + \sigma E_y = -\frac{\partial H_z}{\partial x} \quad (1.b)$$

$$\mu_0 \frac{\partial H_z}{\partial t} + \sigma^* H_z = \frac{\partial E_x}{\partial y} - \frac{\partial E_y}{\partial x} \quad (1.c)$$

Moreover, if the condition

$$\frac{\sigma}{\epsilon_0} = \frac{\sigma^*}{\mu_0} \quad (2)$$

is satisfied, then the impedance of the medium (1) equals that of vacuum and no reflection occurs when a plane wave propagates normally across a vacuum-medium interface. Such a medium is used in the [4-6] technique in order to absorb the outgoing waves.

We will now define the PML medium in the TE case. The cornerstone of this definition is the break of the magnetic component  $H_z$  into two subcomponents which we will denote as  $H_{zx}$  and  $H_{zy}$ . In the TE case, a PML medium is defined as a medium in which the electromagnetic field has

four components,  $E_x$ ,  $E_y$ ,  $H_{zx}$ ,  $H_{zy}$ , connected through the four following equations:

$$\epsilon_0 \frac{\partial E_x}{\partial t} + \sigma_y E_x = \frac{\partial (H_{zx} + H_{zy})}{\partial y} \quad (3.a)$$

$$\epsilon_0 \frac{\partial E_y}{\partial t} + \sigma_x E_y = -\frac{\partial (H_{zx} + H_{zy})}{\partial x} \quad (3.b)$$

$$\mu_0 \frac{\partial H_{zx}}{\partial t} + \sigma_x^* H_{zx} = -\frac{\partial E_y}{\partial x} \quad (3.c)$$

$$\mu_0 \frac{\partial H_{zy}}{\partial t} + \sigma_y^* H_{zy} = \frac{\partial E_x}{\partial y}, \quad (3.d)$$

where the parameters  $(\sigma_x, \sigma_x^*, \sigma_y, \sigma_y^*)$  are homogeneous to electric and magnetic conductivities.

A first remark can be made when looking at system (3). If  $\sigma_x^* = \sigma_y^*$ , then the last two equations can merge and (3) reduces to a set of three equations involving three components  $E_x$ ,  $E_y$ , and  $H_z = H_{zx} + H_{zy}$ . As a result, the PML medium holds as particular cases all the usual media. If  $\sigma_x = \sigma_y = \sigma_x^* = \sigma_y^* = 0$ , (3) reduces to the Maxwell equations of vacuum, if  $\sigma_x = \sigma_y$  and  $\sigma_x^* = \sigma_y^* = 0$ , it reduces to the equations of a conductive medium, and, finally, if  $\sigma_x = \sigma_y$  and  $\sigma_x^* = \sigma_y^*$ , it reduces to the equations of the absorbing medium (1).

A second remark can be made before any calculation. If  $\sigma_y = \sigma_y^* = 0$ , the PML medium can absorb a plane wave  $(E_y, H_{zx})$  propagating along  $x$ , but it does not absorb a wave  $(E_x, H_{zy})$  propagating along  $y$ , since in the first case propagation is ruled by (3.b) and (3.c), and in the second case by (3.a) and (3.d), and vice versa for waves  $(E_y, H_{zx})$  and  $(E_x, H_{zy})$  if  $\sigma_x = \sigma_x^* = 0$ . Such properties of the particular PML media  $(\sigma_x, \sigma_x^*, 0, 0)$  and  $(0, 0, \sigma_y, \sigma_y^*)$  are in close relationship with another one; we will prove later: if their conductivities satisfy (2), then at vacuum-medium interfaces normal respectively to  $x$  and  $y$  these two media do not activate any reflection of electromagnetic waves. Such PML media will be the basis of the PML technique.

### 2.2. Propagation of a Plane Wave in a PML Medium

Let us consider a wave whose electric field of magnitude  $E_0$  forms an angle  $\phi$  with the  $y$  axis (Fig. 1). We will denote as  $H_{zx0}$  and  $H_{zy0}$  the magnitudes of the magnetic components  $H_{zx}$  and  $H_{zy}$ . If a plane wave propagates in the PML medium, then the four components of the field can be expressed as

$$E_x = -E_0 \sin \phi e^{i\omega(t - \alpha x - \beta y)} \quad (4.a)$$

$$E_y = E_0 \cos \phi e^{i\omega(t - \alpha x - \beta y)} \quad (4.b)$$

$$H_{zx} = H_{zx0} e^{i\omega(t - \alpha x - \beta y)} \quad (4.c)$$

$$H_{zy} = H_{zy0} e^{i\omega(t - \alpha x - \beta y)}, \quad (4.d)$$

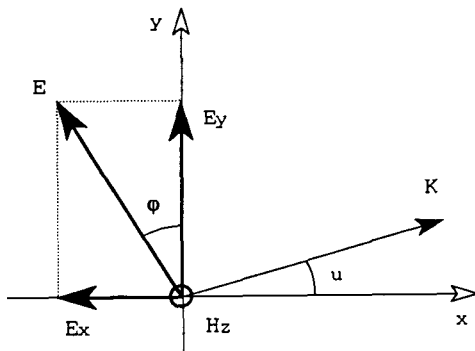


FIG. 1. The transverse electric problem.

where  $\omega$  is the pulsation of the wave,  $t$  is the time, and  $\alpha$  and  $\beta$  are complex constants. Since the magnitude  $E_0$  is given, the set of Eq. (4) involves four unknown quantities to be determined,  $\alpha$ ,  $\beta$ ,  $H_{zx0}$ ,  $H_{zy0}$ . Enforcing  $E_x$ ,  $E_y$ ,  $H_{zx}$ ,  $H_{zy}$  from (4) in the PML equations (3) yields the following set of equations connecting the four unknowns:

$$\varepsilon_0 E_0 \sin \varphi - i \frac{\sigma_y}{\omega} E_0 \sin \varphi = \beta (H_{zx0} + H_{zy0}) \quad (5.a)$$

$$\varepsilon_0 E_0 \cos \varphi - i \frac{\sigma_x}{\omega} E_0 \cos \varphi = \alpha (H_{zx0} + H_{zy0}) \quad (5.b)$$

$$\mu_0 H_{zx0} - i \frac{\sigma_x^*}{\omega} H_{zx0} = \alpha E_0 \cos \varphi \quad (5.c)$$

$$\mu_0 H_{zy0} - i \frac{\sigma_y^*}{\omega} H_{zy0} = \beta E_0 \sin \varphi. \quad (5.d)$$

Obtaining  $H_{zx0}$  and  $H_{zy0}$  from (5.c) and (5.d) and bringing them respectively into (5.a) and (5.b) yields

$$\begin{aligned} \varepsilon_0 \mu_0 \left( 1 - i \frac{\sigma_y}{\varepsilon_0 \omega} \right) \sin \varphi \\ = \beta \left[ \frac{\alpha \cos \varphi}{(1 - i(\sigma_x^*/\mu_0 \omega))} + \frac{\beta \sin \varphi}{(1 - i(\sigma_y^*/\mu_0 \omega))} \right] \end{aligned} \quad (6.a)$$

$$\begin{aligned} \varepsilon_0 \mu_0 \left( 1 - i \frac{\sigma_x}{\varepsilon_0 \omega} \right) \cos \varphi \\ = \alpha \left[ \frac{\alpha \cos \varphi}{(1 - i(\sigma_x^*/\mu_0 \omega))} + \frac{\beta \sin \varphi}{(1 - i(\sigma_y^*/\mu_0 \omega))} \right]. \end{aligned} \quad (6.b)$$

This system of two equations connects the unknowns  $\alpha$  and  $\beta$ . It may be solved by means of writing the ratio (6.a) over (6.b),

$$\frac{\beta}{\alpha} = \frac{\sin \varphi}{\cos \varphi} \frac{1 - i(\sigma_y/\varepsilon_0 \omega)}{1 - i(\sigma_x/\varepsilon_0 \omega)} \quad (7)$$

and then obtaining  $\alpha^2$  from (7) and (6.b) and  $\beta^2$  from (7) and (6.a). That yields two sets of  $(\alpha, \beta)$  of opposite signs for two opposite directions of propagation. Choosing the positive sign we have

$$\alpha = \frac{\sqrt{\varepsilon_0 \mu_0}}{G} \left( 1 - i \frac{\sigma_x}{\varepsilon_0 \omega} \right) \cos \varphi \quad (8.a)$$

$$\beta = \frac{\sqrt{\varepsilon_0 \mu_0}}{G} \left( 1 - i \frac{\sigma_y}{\varepsilon_0 \omega} \right) \sin \varphi, \quad (8.b)$$

where

$$G = \sqrt{w_x \cos^2 \varphi + w_y \sin^2 \varphi} \quad (9)$$

$$w_x = \frac{1 - i(\sigma_x/\varepsilon_0 \omega)}{1 - i(\sigma_x^*/\mu_0 \omega)} \quad (10.a)$$

$$w_y = \frac{1 - i(\sigma_y/\varepsilon_0 \omega)}{1 - i(\sigma_y^*/\mu_0 \omega)}. \quad (10.b)$$

Denoting as  $\Psi$  any component of the field,  $\Psi_0$  its magnitude, and  $c$  the speed of light, with (4) and (8), we can write

$$\psi = \psi_0 e^{i\omega(t - (x \cos \varphi + y \sin \varphi)/cG)} e^{-(\sigma_x \cos \varphi/\varepsilon_0 cG)x} e^{-(\sigma_y \sin \varphi/\varepsilon_0 cG)y}. \quad (11)$$

The last two unknowns  $H_{zx0}$  and  $H_{zy0}$  can be found as functions of  $\alpha$  and  $\beta$  from (5.c) and (5.d), and then enforcing the  $\alpha$  and  $\beta$  values (8) yields

$$H_{zx0} = E_0 \sqrt{(\varepsilon_0/\mu_0)} \frac{1}{G} w_x \cos^2 \varphi \quad (12.a)$$

$$H_{zy0} = E_0 \sqrt{(\varepsilon_0/\mu_0)} \frac{1}{G} w_y \sin^2 \varphi. \quad (12.b)$$

Taking into account (9), the summation of  $H_{zx0}$  and  $H_{zy0}$  is then

$$H_0 = E_0 \sqrt{(\varepsilon_0/\mu_0)} G \quad (13)$$

and the ratio  $Z$  of the electric magnitude over the magnetic one is

$$Z = \sqrt{(\mu_0/\varepsilon_0)} \frac{1}{G}. \quad (14)$$

For formulas (11) and (14), an important occurrence is when both  $(\sigma_x, \sigma_x^*)$  and  $(\sigma_y, \sigma_y^*)$  satisfy the condition (2). Then, the quantities  $w_x$ ,  $w_y$ ,  $G$ , equal unity at any frequency, and so the expression of the wave components (11) and of the impedance (14) become respectively

$$\begin{aligned} \psi = \psi_0 e^{i\omega(t - (x \cos \varphi + y \sin \varphi)/c)} \\ \times e^{-(\sigma_x \cos \varphi/\varepsilon_0 c)x} e^{-(\sigma_y \sin \varphi/\varepsilon_0 c)y} \end{aligned} \quad (15)$$

$$Z = \sqrt{\mu_0/\varepsilon_0}. \quad (16)$$

The first exponential of (15) shows that the wave phase propagates normally to the electric field (that means  $u = \varphi$  on Fig. 1) with the speed of light  $c$ . The last two exponentials rule the magnitude of the wave which decreases exponentially along  $x$  and  $y$ . Formula (16) shows that the impedance of the medium equals that of vacuum. The matching impedance condition (2) of the medium (1) is a matching condition for the PML media too. Differences lie only in the fact that in the case of PML media, two couples

of conductivities must satisfy (2), both  $(\sigma_x, \sigma_x^*)$  and  $(\sigma_y, \sigma_y^*)$ .

Other remarks can be done when looking at (11) or (15). In the general case (11), if a wave propagates along  $y$ , that is,  $\cos \varphi = 0$ , and if, moreover,  $\sigma_y = \sigma_y^* = 0$ , then it is not absorbed. That is in accordance with the second remark achieved after the PML equations (3). In the case of matched media (15), if  $\sigma_y = \sigma_y^* = 0$  the last exponential of (15) equals unity and the absorption is a function of the  $x$  coordinate only.

### 2.3. Transmission of a Wave through PML–PML Interfaces

In this section, we will address the problem of a plane wave moving from a PML medium to another one. We will prove that in particular cases, with adequate sets of parameters  $\sigma_x, \sigma_x^*, \sigma_y, \sigma_y^*$ , the transmission is perfect and reflectionless at any frequency and at any incidence angle. These particular cases will be the basis of the perfectly matched layer.

#### Interface Normal to $x$

We first consider the case of two PML media separated by an interface normal to the  $x$  axis (Fig. 2). Let us denote  $\theta_1$  and  $\theta_2$  the angles of the incident and transmitted electric fields  $E_i$  and  $E_t$ , with respect to the interface plane. As noted after (15) in the previous section, if the media are matched ones  $\theta_1$  and  $\theta_2$  are also the angles that the phase propagation forms with the normal to the interface. Figure 2 is drawn with that assumption. As the  $\varphi$  angle of a PML medium was defined with respect to the  $y$  axis (Fig. 1), in the case of Fig. 2 we have  $\theta = \varphi$  in each media. Let us now assume the interface to be infinite and the incident wave to

be plane. First, both the reflected and transmitted waves must be plane too. Second, the ratios of these waves over the incident one must be without variation when moving on the interface. So, for any component  $\Psi$  of the incident and transmitted fields, and for two points  $A$  and  $B$  of the interface, we can write

$$\frac{\psi_i(B)}{\psi_i(A)} = \frac{\psi_t(B)}{\psi_t(A)}. \quad (17)$$

Denoting as  $d$  the distance from  $A$  to  $B$ , and  $G_1, G_2$  as the quantities (9) of each media, with (11) we have

$$\psi_i(B) = \psi_i(A) e^{-i\omega(d \sin \theta_1 / c G_1) - (\sigma_{y1} \sin \theta_1 / \epsilon_0 c G_1) d} \quad (18.a)$$

$$\psi_t(B) = \psi_t(A) e^{-i\omega(d \sin \theta_2 / c G_2) - (\sigma_{y2} \sin \theta_2 / \epsilon_0 c G_2) d}. \quad (18.b)$$

Since (17) is true for any distance  $d$ , the exponential factors of (18.a) and (18.b) must be equal. So the relation

$$\left(1 - i \frac{\sigma_{y1}}{\epsilon_0 \omega}\right) \frac{\sin \theta_1}{G_1} = \left(1 - i \frac{\sigma_{y2}}{\epsilon_0 \omega}\right) \frac{\sin \theta_2}{G_2}, \quad (19.a)$$

must be satisfied, where

$$G_k = \sqrt{w_{xk} \cos^2 \theta_k + w_{yk} \sin^2 \theta_k} \quad (\text{for } k = 1, 2). \quad (19.b)$$

This relation, which connects the incident and transmitted angles, is the Snell–Descartes law at an interface normal to  $x$ , lying between two PML  $(\sigma_x, \sigma_x^*, \sigma_y, \sigma_y^*)$  media. The demonstration related to the transmitted wave could be reproduced for the reflected one, with the conclusion that the reflected angle equals  $\pi - \theta_1$ .

Let us now consider the incident, reflected, and transmitted electric and magnetic fields  $E_i, E_r, E_t, H_i, H_r, H_t$  (Fig. 2). First, continuity of the fields  $E_y$  and  $H_{zx} + H_{zy}$  lying in the interface yields the following set of equations:

$$E_i \cos \theta_1 - E_r \cos \theta_1 = E_t \cos \theta_2 \quad (20.a)$$

$$H_i + H_r = H_t. \quad (20.b)$$

Second, denoting as  $E_{i0}, E_{r0}, E_{t0}$ , the magnitudes of  $E_i, E_r, E_t$ , and setting  $x = 0$  in the interface, with (11) and (14) we can write

$$E_i = E_{i0} e^{-i\omega(y \sin \theta_1 / c G_1)(1 - i(\sigma_{y1}/\epsilon_0 \omega))} e^{i\omega t} \quad (21.a)$$

$$E_r = E_{r0} e^{-i\omega(y \sin \theta_1 / c G_1)(1 - i(\sigma_{y1}/\epsilon_0 \omega))} e^{i\omega t} \quad (21.b)$$

$$E_t = E_{t0} e^{-i\omega(y \sin \theta_2 / c G_2)(1 - i(\sigma_{y2}/\epsilon_0 \omega))} e^{i\omega t} \quad (21.c)$$

$$H_i = E_i / Z_1, \quad H_r = E_r / Z_1, \quad H_t = E_t / Z_2. \quad (21.d), (21.e), (21.f)$$

As a consequence of the Snell–Descartes law (19), the three exponentials on space of (21.a), (21.b), (21.c) are equal. So,

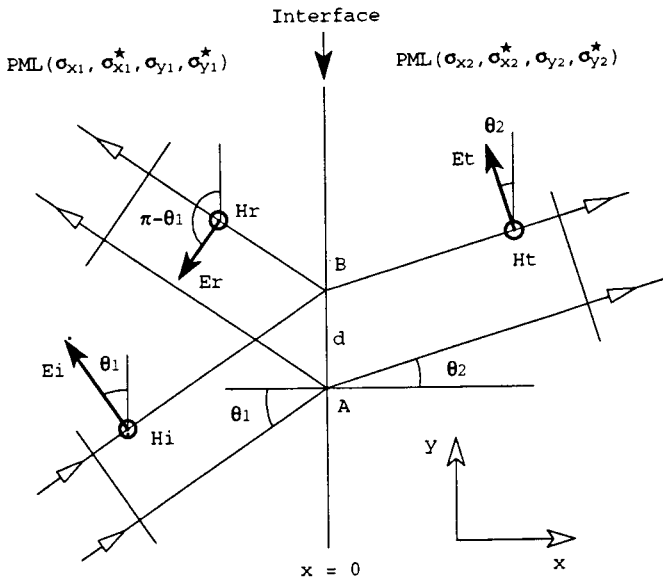


FIG. 2. Interface lying between two PML media.

reporting  $E_i, \dots, H_i$  from (21) into (20), this system (20) becomes

$$E_{i0} \cos \theta_1 - E_{r0} \cos \theta_1 = E_{t0} \cos \theta_2 \quad (22.a)$$

$$\frac{E_{i0}}{Z_1} + \frac{E_{r0}}{Z_1} = \frac{E_{t0}}{Z_2}. \quad (22.b)$$

Defining the reflection factor as the ratio of the electric components lying in the interface, that is,  $-E_{r0} \cos \theta_1 / E_{i0} \cos \theta_1$ , and then solving the set (22) for this ratio, the reflection factor  $r_p$  for the TE case is

$$r_p = \frac{Z_2 \cos \theta_2 - Z_1 \cos \theta_1}{Z_2 \cos \theta_2 + Z_1 \cos \theta_1}. \quad (23)$$

This factor (23) is as at an interface lying between two usual media. The formula for the transmission factor would be the same as usual, too. With (14), we can rewrite (23) as

$$r_p = \frac{G_1 \cos \theta_2 - G_2 \cos \theta_1}{G_1 \cos \theta_2 + G_2 \cos \theta_1}, \quad (24)$$

where  $G_1$  and  $G_2$  are functions of  $\theta_1$  and  $\theta_2$  through (19.b).

We will now address a particular case announced at the beginning of this section. Let us consider an interface lying between media having same  $\sigma_y$  and  $\sigma_y^*$  conductivities, that is, a  $(\sigma_{x1}, \sigma_{x1}^*, \sigma_y, \sigma_y^*)$  and a  $(\sigma_{x2}, \sigma_{x2}^*, \sigma_y, \sigma_y^*)$  media. Then the Snell-Descartes law (19.a) becomes

$$\frac{\sin \theta_1}{G_1} = \frac{\sin \theta_2}{G_2}. \quad (25)$$

If, moreover, the two media are matched ones, that is,  $(\sigma_{x1}, \sigma_{x1}^*), (\sigma_{x2}, \sigma_{x2}^*)$ , and  $(\sigma_y, \sigma_y^*)$  satisfying (2), we have  $G_1 = G_2 = 1$ , so (25) reduces to

$$\theta_1 = \theta_2 \quad (26)$$

and the reflection factor (24) is then

$$r_p = 0. \quad (27)$$

So, at an interface normal to  $x$  lying between two matched PML media having the same  $(\sigma_y, \sigma_y^*)$ , a plane wave is transmitted without reflection at any incidence angle and at any frequency. That is also true, of course, if the first medium is a vacuum and the second one is a  $(\sigma_x, \sigma_x^*, 0, 0)$  medium, since a vacuum can be seen as a  $(0, 0, 0, 0)$  medium.

In the general case of unmatched media having the same  $(\sigma_y, \sigma_y^*)$ , a simple formula can be obtained for the factor (24). Bringing (25) into (24) yields

$$r_p = \frac{\sin \theta_1 \cos \theta_2 - \sin \theta_2 \cos \theta_1}{\sin \theta_1 \cos \theta_2 + \sin \theta_2 \cos \theta_1}. \quad (28)$$

Then, squaring (25), replacing  $G_1$  and  $G_2$  by (19.b), and taking into account that  $w_{y1} = w_{y2}$ , we can deduce that

$$\sqrt{w_{x2}} \sin \theta_1 \cos \theta_2 = \sqrt{w_{x1}} \sin \theta_2 \cos \theta_1 \quad (29)$$

and with (28) and (29),

$$r_p = \frac{\sqrt{w_{x1}} - \sqrt{w_{x2}}}{\sqrt{w_{x1}} + \sqrt{w_{x2}}}. \quad (30)$$

Formula (30) shows that even if the media are not matched ones, the reflection does not depend on the incidence angle  $\theta_1$ . It depends only on the frequency through (10). In the case of matched media  $w_{x1} = w_{x2} = 1$  and (30) reduces to (27) as expected.

#### Interface Normal to $y$

Let us consider a plane wave propagating upward and striking an interface normal to the  $y$  axis. Defining the incidence angle  $\theta$  as in the previous case with respect to the interface, since  $\varphi$  is defined with respect to the  $y$  axis (Fig. 1) we have now  $\varphi = \theta + \pi/2$ . Similar treatment as in the previous case yields then the Snell-Descartes law related to an interface normal to  $y$ ,

$$\left(1 - i \frac{\sigma_{x1}}{\varepsilon_0 \omega}\right) \frac{\sin \theta_1}{G_1} = \left(1 - i \frac{\sigma_{x2}}{\varepsilon_0 \omega}\right) \frac{\sin \theta_2}{G_2}, \quad (31.a)$$

where

$$G_k = \sqrt{w_{xk} \sin^2 \theta_k + w_{yk} \cos^2 \theta_k} \quad (\text{for } k = 1, 2). \quad (31.b)$$

In the case of two media having the same  $\sigma_x$  and  $\sigma_x^*$ , (31.a) becomes (25). If, moreover, these media are matched ones, then  $G_1 = G_2$  and (31.a) reduces to (26). Since the reflection factor is still (23), (27) is still true. So, at an interface normal to  $y$  lying between two matched media having the same  $(\sigma_x, \sigma_x^*)$ , the reflection factor is always null.

#### Practical Conclusions of This Section

As a summary of this section we can now say that the reflection factor between two PML media whose conductivities satisfy (2) is null:

- at an interface normal to  $x$  in the case of the same  $\sigma_y$  and  $\sigma_y^*$ .
- at an interface normal to  $y$  in the case of the same  $\sigma_x$  and  $\sigma_x^*$ .

This result is, of course, true if some conductivities equal zero. Having in mind that a vacuum is a  $(0, 0, 0, 0)$  PML medium, each of the previous cases yields two particular occurrences which will be the basis of the PML technique. These occurrences are

— the reflection factor is null at an interface normal to  $x$  lying between a vacuum and a  $(\sigma_x, \sigma_x^*, 0, 0)$  matched medium or between a  $(0, 0, \sigma_y, \sigma_y^*)$  and a  $(\sigma_x, \sigma_x^*, \sigma_y, \sigma_y^*)$  matched media.

— the reflection factor is null at an interface normal to  $y$  lying between a vacuum and a  $(0, 0, \sigma_y, \sigma_y^*)$  matched medium or between a  $(\sigma_x, \sigma_x^*, 0, 0)$  and a  $(\sigma_x, \sigma_x^*, \sigma_y, \sigma_y^*)$  matched media.

#### 2.4. Perfectly Matched Layer for the Finite Difference Technique

The general frame of the PML technique is pointed out on Fig. 3. The Maxwell equations are solved by the FDTD (finite-difference time-domain) technique [1, 11] inside a computational domain in which lies a source of outgoing waves. For instance, such a source will be the scatterer in a wave-structure interaction problem. The computational domain is surrounded by an absorbing layer which is an aggregate of PML media whose properties have been predicted in previous sections. The domain is finally ended by perfectly conducting conditions.

On both the left and right sides of the computational domain, the absorbing layers are matched PML  $(\sigma_x, \sigma_x^*, 0, 0)$  media. So, at interfaces vacuum-layer AB and CD normal to the  $x$  axis, the reflection factor is theoretically null, as it has been proved (Eq. (27)). Outgoing waves can propagate without reflection through the AB and CD interfaces. Similarly, matched PML  $(0, 0, \sigma_y, \sigma_y^*)$  media are used on both upper and lower sides of the computational domain so that the outgoing waves can propagate without reflection

through the BC and DA interfaces normal to  $y$ . At the four corners of the domain, the absorbing layers are made of PML  $(\sigma_x, \sigma_x^*, \sigma_y, \sigma_y^*)$  media having conductivities equal to those of the adjacent  $(\sigma_x, \sigma_x^*, 0, 0)$  and  $(0, 0, \sigma_y, \sigma_y^*)$  media. As a result, there is theoretically no reflection at the interfaces lying between the side layers and the corner layers. For instance, a wave can propagate without reflection through the BB<sub>1</sub> and BB<sub>2</sub> interfaces of Fig. 3.

As physical remark, we can note that with the PML layer, the speed of propagation is the speed of light in the whole computational domain, and the Snell–Descartes law is (26) at all interfaces. So, as a wave travels from a medium to another one through interfaces, its shape is preserved. That is in close relationship with the lack of reflection at interfaces.

In the absorbing layer, the magnitude of a wave is ruled by the last two exponential factors of (15). In the side layers which are  $(\sigma_x, \sigma_x^*, 0, 0)$  or  $(0, 0, \sigma_y, \sigma_y^*)$  media, one factor equals unity. So, at a distance  $\rho$  of any interface, the magnitude of an outgoing plane wave can be written as

$$\psi(\rho) = \psi(0) e^{-(\sigma \cos \theta / \epsilon_0 c) \rho}, \quad (32)$$

where  $\theta$  is the incidence angle defined with respect to the interface, and  $\sigma$  is either  $\sigma_x$  or  $\sigma_y$ . After crossing the layer, a wave is reflected by the perfectly conducting conditions which ends the domain, and then, after a second crossing, it can come back into the vacuum. So, for a layer of thickness  $\delta$ , an apparent reflection factor can be defined as

$$R(\theta) = e^{-2(\sigma \cos \theta / \epsilon_0 c) \delta}. \quad (33)$$

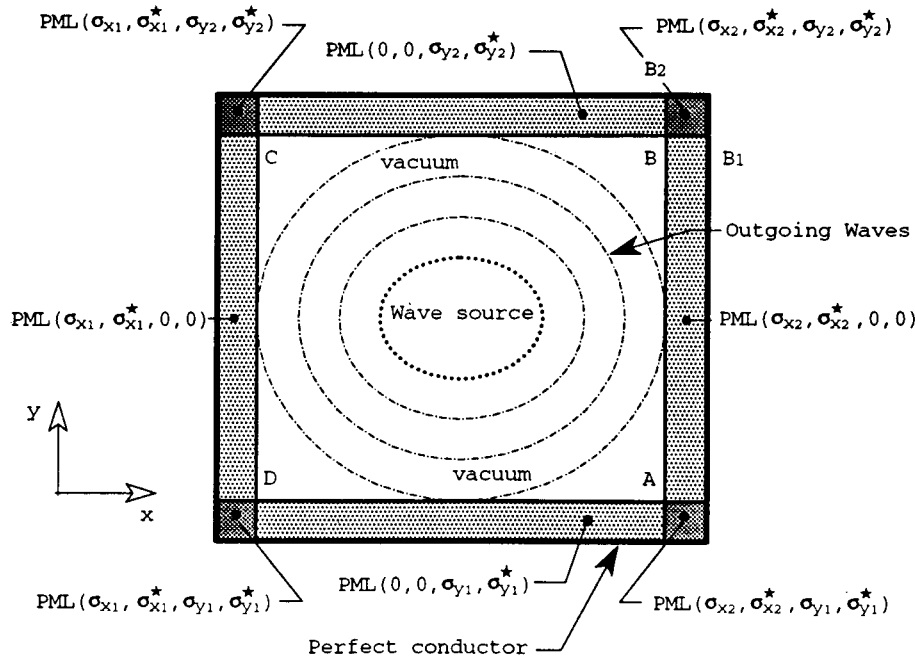


FIG. 3. The PML technique.

This formula claims a remark. If the incident wave is close to the interface ( $\theta \sim \pi/2$ ) the factor  $R$  is close to unity, whatever  $\sigma$  may be. This is not troublesome in practical computations as we will see from numerical tests. It is not surprising, indeed, since for instance, a close to the interface wave on the right side of the domain will come perpendicularly to the upper (or lower) side, where it will be absorbed.

As (33) points out, the apparent reflection is a function of the product  $\sigma\delta$ . So, for a given layer attenuation, theoretically the layer thickness  $\delta$  could be as thin as intended, reduced to one cell of the FDTD mesh, for instance. In fact, sharp variations of conductivity create numerical reflections, as with the [4–6] technique. So, in practical computations the layer has to be a few cells thick with conductivity increasing from zero at the vacuum–layer interface to a value  $\sigma_m$  at the outer side of the layer. For a conductivity  $\sigma(\rho)$  the reflection factor is then

$$R(\theta) = e^{-2(\cos \theta/\epsilon_0 c) \int_0^\delta \sigma(\rho) d\rho}. \quad (34)$$

All numerical computations reported in this paper have been performed with conductivities of the form

$$\sigma(\rho) = \sigma_m \left( \frac{\rho}{\delta} \right)^n \quad (35)$$

for which, enforcing (35) in (34), the apparent reflection is

$$R(\theta) = e^{-(2/(n+1))(\sigma_m \delta/\epsilon_0 c) \cos \theta}. \quad (36)$$

Numerical implementation of the PML layer in the FDTD technique does not involve special treatment. Let us consider, for instance, the upper-right part of a gridded computational domain (Fig. 4). In the layer, the equations

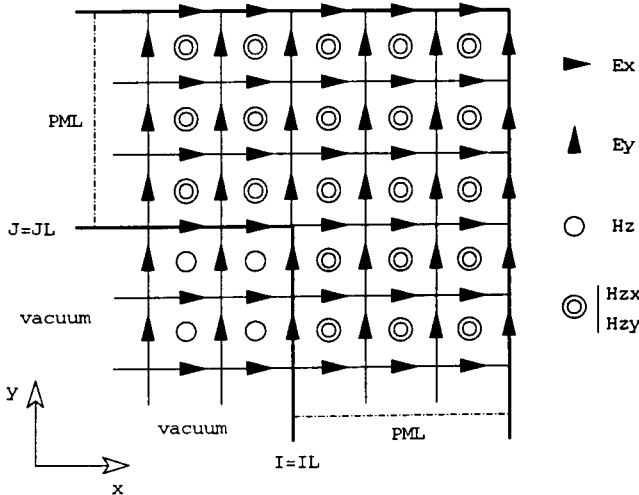


FIG. 4. Upper-right part of the FDTD grid.

to be discretized are (3). In the inner volume (vacuum and scattering structure, for instance) the set (3) could be used too, since the usual media can be seen as particular PML media. But having in mind computer storage optimization, it is more convenient to use the Maxwell equations which address only three field components, instead of four, with (3).

In the inner volume (for  $I < IL$  and  $J < JL$  on Fig. 4) the finite-difference equations are the usual [1, 11] discretizations of the Maxwell equations. In the PML medium, the two magnetic subcomponents are computed at the same points, in place of the magnetic component  $H_z$ . Discretization of the set (3) is straightforward. With the usual FDTD notations, (3.b) and (3.c) yield the following equations that can be applied in the whole layer, except in the interface for  $E_y$  (see below),

$$\begin{aligned} E_y^{n+1}(i, j+1/2) &= e^{-\sigma_x(i) \Delta t/\epsilon_0} E_y^n(i, j+1/2) - \frac{(1 - e^{-\sigma_x(i) \Delta t/\epsilon_0})}{\sigma_x(i) \Delta x} \\ &\times [H_{zx}^{n+1/2}(i+1/2, j+1/2) + H_{zy}^{n+1/2}(i+1/2, j+1/2) \\ &- H_{zx}^{n+1/2}(i-1/2, j+1/2) - H_{zy}^{n+1/2}(i-1/2, j+1/2)] \end{aligned} \quad (37)$$

$$\begin{aligned} H_{zx}^{n+1/2}(i+1/2, j+1/2) &= e^{-\sigma_x^*(i+1/2) \Delta t/\mu_0} H_{zx}^{n-1/2}(i+1/2, j+1/2) \\ &- \frac{(1 - e^{-\sigma_x^*(i+1/2) \Delta t/\mu_0})}{\sigma_x^*(i+1/2) \Delta x} \\ &\times [E_y^n(i+1, j+1/2) - E_y^n(i, j+1/2)], \end{aligned} \quad (38)$$

where  $\sigma_x$  and  $\sigma_x^*$  are functions of  $x(I)$ , in the left, right, and corner layers, and are equal to zero, in the upper and lower layers (for  $I < IL$  on Fig. 4). For the  $E_y$  component lying in the interface, the magnetic field has one component  $H_z$  on one side and two subcomponents  $H_{zx}$ ,  $H_{zy}$  on the other. That is a result of using the Maxwell equations in the inner volume, but it has no physical significance ( $H_{zx}$  and  $H_{zy}$  are present in the inner volume where they merge, since  $\sigma_x^*$  equals  $\sigma_y^*$ ). The finite difference equations have to be modified. So, in the right side interface normal to  $x$ , (37) becomes

$$\begin{aligned} E_y^{n+1}(il, j+1/2) &= e^{-\sigma_x(il) \Delta t/\epsilon_0} E_y^n(il, j+1/2) - \frac{(1 - e^{-\sigma_x(il) \Delta t/\epsilon_0})}{\sigma_x(il) \Delta x} \\ &\times [H_{zx}^{n+1/2}(il+1/2, j+1/2) + H_{zy}^{n+1/2}(il+1/2, j+1/2) \\ &- H_{zx}^{n+1/2}(il-1/2, j+1/2)]. \end{aligned} \quad (39)$$

In all computations of this paper, conductivities which depend on index  $I$  (or  $J$ , too) were implemented as the

average value in the cell around the index location. That can be written for  $\sigma_x(I)$ ,

$$\sigma_x(i) = \frac{1}{\Delta x} \int_{x(i) - \Delta x/2}^{x(i) + \Delta x/2} \sigma_x(x') dx', \quad (40)$$

where  $\sigma_x(x)$  was of the form (35) in our computations.

The discretized equations needed for the advance of the components  $E_x$  and  $H_{zy}$  are obtained from the remaining equations (3.a) and (3.d). That yields three equations analogous to (37), (38), (39).

### 2.5. PML Medium for the Transverse Magnetic Case

In TM problems, the electromagnetic field reduces to three components,  $E_z$ ,  $H_x$ ,  $H_y$ . In a PML medium, the component which is split into two subcomponents is the electric field  $E_z$ . The PML medium equations for the TM case are the following:

$$\epsilon_0 \frac{\partial E_{zx}}{\partial t} + \sigma_x E_{zx} = \frac{\partial H_y}{\partial x} \quad (41.a)$$

$$\epsilon_0 \frac{\partial E_{zy}}{\partial t} + \sigma_y E_{zy} = -\frac{\partial H_x}{\partial y} \quad (41.b)$$

$$\mu_0 \frac{\partial H_x}{\partial t} + \sigma_y^* H_x = -\frac{\partial (E_{zx} + E_{zy})}{\partial y} \quad (41.c)$$

$$\mu_0 \frac{\partial H_y}{\partial t} + \sigma_x^* H_y = \frac{\partial (E_{zx} + E_{zy})}{\partial x}. \quad (41.d)$$

Same calculations as in the TE case yield slightly changed results. In most formulas, especially in (8), (10), (19.a), (19.b), the change is only a permutation of  $\epsilon_0$  with  $\mu_0$  and of starred  $\sigma$  with unstarred ones. In (14),  $1/G$  is changed to  $G$  and (23) has to be replaced by the usual  $r_s$  factor. But the most important result is left unchanged. As in the TE case, there is no reflection both at an interface normal to  $x$  between two matched media having the same  $(\sigma_y, \sigma_y^*)$  and at an interface normal to  $y$  between two matched media having the same  $(\sigma_x, \sigma_x^*)$ . So, an absorbing reflectionless layer can be built as in the TE case.

## 3. NUMERICAL EXPERIMENTS

In order to evaluate the actual possibilities of the PML technique in practical computations, six numerical experiments are presented here. The first two are elementary tests which compare the theoretical reflection factor with its practical counterpart when a plane wave strikes either an infinite vacuum-layer interface or the corner of a computational domain. The third experiment is related to the absorption of a pulse on the boundaries of a computational domain. The last three are closer to some realistic applica-

tions. We will consider successively a wave-structure interaction problem in the TE case, a wave-structure interaction problem in the TM case, and finally the problem of a slot radiating in free space.

### 3.1. Techniques Used for Numerical Comparisons

In most numerical experiments, the results were computed with both the PML technique and three other techniques of free-space simulation in order to evaluate the improvement we can expect from using the PML technique. The first technique used in these comparisons was the matched layer [4–6] which we will refer to as ML on the figures. The second technique was the one-way wave equation in its Padé approximation version. Discretization was the same as in [8, 10] for the first two orders of approximation. Some results were also computed with the third order using a discretization of our own. We will refer to this technique as one-way on the figures. The third technique, referred to as operator, is that of Higdon operators defined directly in finite-difference terms. We used the following operator, which is a particular case of the general operator addressed in [9],

$$B(K, Z^{-1}) = \left[ I - KZ^{-1} + \frac{\Delta x - c \Delta t}{\Delta x + c \Delta t} (K - Z^{-1}) \right]^p, \quad (42)$$

where  $I$ ,  $K$ ,  $Z^{-1}$  are the identity and shift operators of [9] and  $p$  is the order of the operator (2 or 3 in our computations).

For the one-way and operator techniques, the reflection factor of a plane wave is, at an incidence angle  $\theta$ ,

$$R(\theta) = \left( \frac{1 - \cos \theta}{1 + \cos \theta} \right)^p. \quad (43)$$

For the ML technique, with conductivities to be used in order to absorb the outgoing waves over a few cells of the FDTD mesh [5], the practical reflection factor is also (43) with  $p = 1$ .

### 3.2. Reflection of a Plane Wave Striking a Plane Boundary

As the first finite difference experiment, we have computed the reflection factor of a plane wave striking a plane boundary, in the TE case. Figure 5 shows the computational domain used. The boundary to be tested is applied on one side of the domain in which a plane wave is produced by the Huyghens surface technique [6]. Both the incident wave and the reflected one are present inside the Huyghens surface, but only the reflected wave is outside it. So, the reflected wave is obtained at a point P close to this surface but outside it. As it appears on Fig. 5, the computation is correct only during a clear time which depends on the



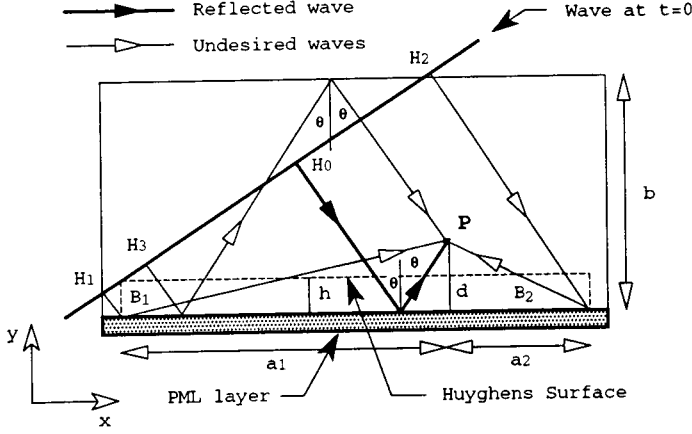


FIG. 5. FDTD domain for computing the reflection of a plane wave.

dimensions of the domain. Three undesired fields disturb the desired result at P, first, the non-physical artefacts coming from  $B_1$  and  $B_2$ , where the Huyghens surface is broken, and, second, the wave reflected on the boundary to be tested, and on the upper side of the domain. Setting the beginning of computation when the wave is just striking the corner of the Huyghens surface (Fig. 5), the reflected wave will arrive at a time  $t_0$ , whereas the undesired fields will arrive at times  $t_1, t_2, t_3$ . With the distances defined on Fig. 5, some calculations yield the following times:

$$ct_0 = h \cos \theta + a_1 \sin \theta + d \cos \theta \quad (44.a)$$

$$ct_1 = ct_0 + \sqrt{a_1^2 + d^2} - a_1 \sin \theta - d \cos \theta \quad (44.b)$$

$$ct_2 = ct_0 + \sqrt{a_2^2 + d^2} + a_2 \sin \theta - d \cos \theta \quad (44.c)$$

$$ct_3 = ct_0 + 2(b - d) \cos \theta \quad (44.d)$$

In practical computations,  $t_1, t_2, t_3$ , are set in order to have a desired clear time, and then (44.b), (44.c), (44.d) yield the dimensions  $a_1, a_2, b$  of the domain.

Computations have been performed with a  $5 \times 5$ -cm cell and a 0.1-ns time step. The incident wave was a Gaussian pulse of 1 ns time constant, and the reflection factor was computed by means of a Fourier transformation of the reflected pulse observed during the clear time at P. The Huyghens surface and P were set respectively 3 and 5 cells from the boundary. Calculations have been performed from normal to  $75^\circ$  incidences, within domains varying from  $300 \times 80$  to  $2000 \times 130$  cells so that the clear times were in the interval 100–200 time steps (10–20 ns). The resolution of the Fourier transformation was then better than 100 Mhz. We used as reflection factors the values obtained from the low frequency limit of the Fourier transformation of the reflected pulse. So, these factors were actually reflection factors around the 100-MHz resolution, at frequencies only slightly disturbed by the FDTD mesh, whose cutoff is about 100 times higher.

TABLE I

Reflection Factor (%) for a Plane Wave Striking a Plane Boundary

Boundary conditions	$\theta = 0$	$\theta = 45^\circ$	$\theta = 75^\circ$
	FDTD * theory	FDTD * theory	FDTD * theory
One-way 2	0.010 * 0.000	2.945 * 2.944	34.67 * 34.67
Operator 2	0.003 * 0.000	2.945 * 2.944	34.67 * 34.67
One-way 3	0.001 * 0.000	0.505 * 0.505	20.41 * 20.41
PML(4, C, 1.0)	3.053 * 1.000	4.953 * 3.853	30.53 * 30.36
PML(4, L, 1.0)	1.080 * 1.000	3.991 * 3.853	30.42 * 30.36
PML(4, L, 0.1)	0.059 * 0.100	0.820 * 0.756	16.84 * 16.73
PML(4, L, 0.01)	0.133 * 0.010	0.126 * 0.148	9.358 * 9.220
PML(4, P, 0.01)	0.041 * 0.010	0.234 * 0.148	9.437 * 9.220
PML(4, P, 0.001)	0.012 * 0.001	0.073 * 0.029	5.317 * 5.080
PML(8, P, 0.001)	0.0015 * 0.001	0.038 * 0.029	5.158 * 5.080
PML(8, P, 0.0001)	0.0010 * 0.0001	0.0085 * 0.0057	2.873 * 2.800
Missmatched PML	17.16 * 17.16	17.16 * 17.16	17.15 * 17.16
ML(4, L, 0.1)	0.059 * 0.100	17.10 * 17.16	58.90 * 58.88

Table I presents some results for three incidence angles and various boundary conditions. In each case two values of the reflection factor expressed as percentages are reported. The first value was computed by the FDTD technique and the second one, by the theoretical formula which is either (36) for the PML layer or (43) for the other techniques. The first three lines of the table are related to the one-way and operator techniques, with both second and third orders. One can see that the FDTD results are in very sharp agreement with the theoretical formula (43) at oblique incidences, and that the reflection is very short at normal incidence. The next eight lines are related to eight different PML layers. In Table I and always in this paper, a PML layer is defined by three parameters. The first one is the number of cells. The second one is a letter which means the variation of the conductivity, a C for constant conductivity, a L for linear conductivity, or a P for parabolic conductivity (in (35),  $n = 0, 1, 2$ , respectively). The last parameter is the theoretical reflection at normal incidence  $R(0)$ , expressed as a percentage. This factor  $R(0)$  is related to the conductivity  $\sigma_m$  defined in (35) since (36) can be rewritten as

$$R(\theta) = [R(0)]^{\cos \theta} \quad (45)$$

with

$$R(0) = e^{-(2/(n+1))(\sigma_m \delta / \epsilon_0 c)}. \quad (46)$$

Table I gives results for PML layers both four and eight cells thick. The first PML result is for a constant conductivity with  $R(0)$  equal to 1%. In this case the reflection factor computed by FDTD is about in accordance with its theoretical value (45) at oblique incidences, but it is three times its theoretical value at normal incidence. So, a con-

stant conductivity produces a strong numerical reflection at the vacuum-layer interface. This reflection is widely reduced when using a linear conductivity, as the next three cases of Table I show. Then, the FDTD factors are in good agreement with their theoretical values when  $R(0)$  equals both 1 and 0.1%. Numerical reflection appears only when  $R(0)$  equals 0.01%, for which the normal reflection is greater than that observed when  $R(0)$  equals 0.1%. As the last two four-cells PML layers of Table I show, a larger reduction of numerical reflection can be obtained from using a parabolic conductivity. Then the FDTD factor is reduced to about 0.01% at normal incidence when  $R(0)$  equals 0.001%. Finally, the last two PML layers of Table I show that another way to reduce the amount of numerical reflection is to increase the thickness of the layer. With an eight-cell parabolic layer, the reflection at normal incidence is reduced to 0.001% when using  $R(0)$  equal to 0.0001%. Such a  $R(0)$  value allows very short reflection at high incidence angles, less than 3% at  $75^\circ$ .

For normal and  $45^\circ$  incidences, three conductivity variations, and four-cell layers, Fig. 6 presents the FDTD reflection factor as a function of the theoretical factor  $R(0)$ . This figure confirms the results of Table I, with a constant conductivity the FDTD reflection cannot be shorter than 3%,

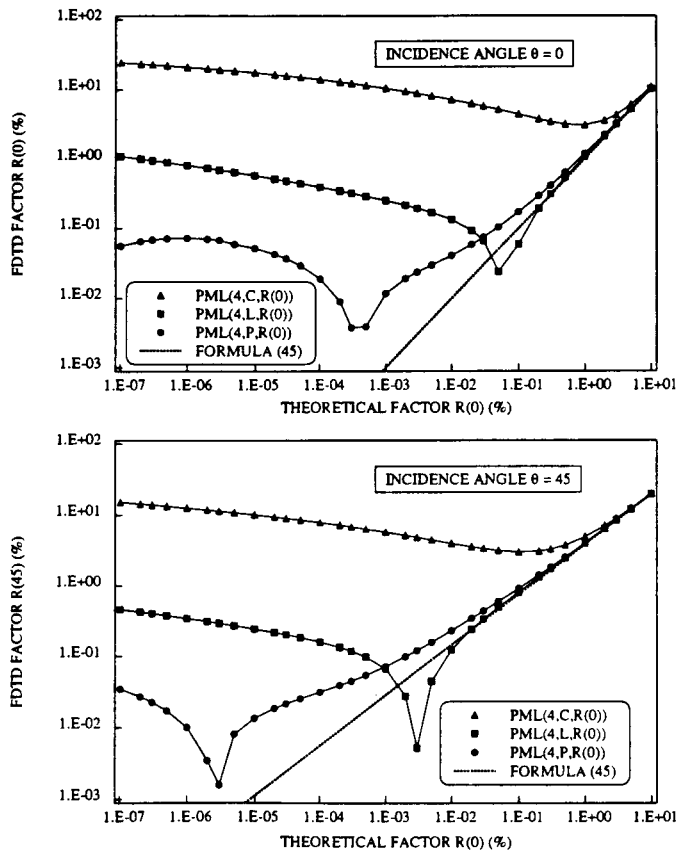


FIG. 6. FDTD reflection factor as a function of the theoretical reflection factor  $R(0)$  for two incidence angles.

while with respectively linear and parabolic conductivities it can be of the order of 0.1 and 0.01%. Moreover, we can see that in all cases, under an optimum value of  $R(0)$ , that reflection rises in the vicinity of the normal incidence. With a parabolic conductivity, for instance, this optimum is in the range 0.001 to 0.0001%.

For a parabolic conductivity, Fig. 7 gives the reflection factor as a function of the incidence angle. As suggested by Fig. 6, the FDTD factor is close to its theoretical counterpart at high incidence angles. Numerical reflection appears above all in the vicinity of the normal incidence, where the theoretical reflection is short. What appears clearly on Fig. 7 is that the practical reflection can be far shorter than that of the second-order one-way technique, in most of the incidence angle range. At incidence  $45^\circ$  the PML reflection is then about 100 times shorter when using an  $R(0)$  factor around 0.0001%.

The next to last line of Table I gives the reflection factor computed with a PML medium which does not satisfy the matching condition (2). Computations have been performed with a highly absorbing layer in order to have an apparent reflection (45) that is negligible at the incidences of interest and, then, to observe only the reflection at the vacuum-layer interface. The results of Table I were obtained using a PML(15, L, 1.E-10) medium whose conductivity  $\sigma_m$  was set to its normal value 0.098 mho yielded by (46), but whose magnetic conductivity  $\sigma_m^*$  was set to two times the value deduced from (2). At frequencies around 100 MHz, with (10) we had  $w_x = \frac{1}{2}$  and, then, the theoretical reflection factor (30) at the vacuum-layer interface was equal to 17.16%. The results of the FDTD computation reported in Table I are in sharp agreement with that prediction and, especially, the reflection does not depend on the incidence angle.

The last line of Table I gives the reflection factor computed with the ML technique [4-6], a linear conduc-

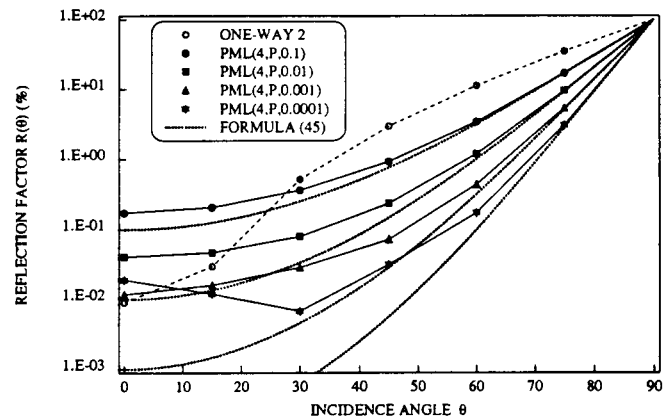


FIG. 7. FDTD reflection factors as functions of the incidence angle, for four-cell parabolic layers. These factors are compared with their theoretical counterparts given by formula (45) and with the FDTD reflection factor of the second-order one-way technique.

tivity, and a 0.1 % apparent reflection at normal incidence. As expected, at oblique incidences the reflection factor is in accordance with the first order of formula (43).

In conclusion, what appears along these first numerical experiments is that the theoretical properties of the PML layer are preserved in the FDTD computations. A small amount of numerical reflection appears at the vacuum-layer interface, but with a magnitude that can be controlled while tuning some parameters of the PML layer, mainly its conductivity profile and number of cells. So, in practical computations, very short FDTD reflection factors can be obtained using the PML technique. For instance, with a PML layer having four cells only, the actual reflection factor can be widely shorter than that of the second order one-way technique.

### 3.3. Reflection of a Plane Wave Striking a Computational Domain Corner

In order to check that at the corners of a computational domain the absorption of waves is in accordance with the theory of the PML technique, we have performed numerical tests with the domain of Fig. 8. Either the absorbing layer or another boundary condition is set on two sides of the domain in which a plane wave is produced by a Huygens surface. At a point P outside this surface, the field is the summation of three waves. The first one is reflected on the boundary normal to  $y$ , the second one on the boundary normal to  $x$ , and the third one on the two boundaries. Since in PML media the shape of waves coming from vacuum is preserved, the reflected components of the field are set as if they were reflected by the conducting planes ending the domain. So, for P close to the corner, so that the phase-shift between the three reflected waves can be neglected, one can

deduce the ratios of the reflected components at P over the incident ones,

$$E_x/E_{xi} = R(\pi/2 - \theta) - R(\theta) - R(\theta) R(\pi/2 - \theta) \quad (47.a)$$

$$E_y/E_{yi} = R(\theta) - R(\pi/2 - \theta) - R(\theta) R(\pi/2 - \theta) \quad (47.b)$$

$$H_z/H_{zi} = R(\theta) + R(\pi/2 - \theta) + R(\theta) R(\pi/2 - \theta), \quad (47.c)$$

where  $R(\theta)$  is the magnitude of the reflection factor (45), and  $\theta$  is the incidence defined on Fig. 8. The formulas (47) are also valid for both one-way and operator conditions, with the reflection factor (43) in place of (45).

As in the case of reflection on a plane boundary, the computation is exact during a clear time only. Two non-physical fields will disturb the result at P, coming from B1 and B2, where the Huygens surface is broken. Setting the beginning of computation when the incident wave is just striking the Huyghens surface (Fig. 8) and, since P is close to the corner (5 cells), the times  $t_0$ ,  $t_1$ ,  $t_2$  at which the reflected wave and the undesired fields will arrive at P can be approximated as

$$ct_0 = a \sin \theta \quad (48.a)$$

$$ct_1 = ct_0 + a(1 - \sin \theta) \quad (48.b)$$

$$ct_2 = ct_0 + b(1 - \cos \theta). \quad (48.c)$$

Computations have been performed with 5 \* 5-cm cells and a 0.1-ns time step. The results reported in Table II for 45° and 75° incidence angles were obtained within 300 \* 300 and 2000 \* 120 computational domains, allowing clear times greater than 10 ns.

TABLE II

Reflected Field (%) near a Computational Corner

Boundary conditions	$E_x/E_{xi}$ FDTD * theory	$E_y/E_{yi}$ FDTD * theory	$H_z/H_{zi}$ FDTD * theory
Incidence angle $\theta = 45^\circ$			
One-way 1	2.942 * 2.944	2.942 * 2.944	37.26 * 37.26
One-way 2	16.13 * 0.087	16.13 * 0.087	18.48 * 5.974
Operator 2	0.087 * 0.087	0.087 * 0.087	5.977 * 5.974
PML(4, L, 1.0)	0.158 * 0.148	0.158 * 0.148	8.141 * 7.854
PML(4, L, 0.01)	1.7E-3 * 2.2E-4	1.7E-3 * 2.2E-4	0.251 * 0.297
PML(4, P, 0.001)	1.5E-3 * 8.5E-6	1.5E-3 * 8.9E-6	0.146 * 0.058
Incidence angle $\theta = 75^\circ$			
One-way 1	58.16 * 58.17	56.13 * 56.13	61.64 * 61.63
One-way 2	49.97 * 34.65	30.67 * 34.63	39.04 * 34.71
Operator 2	34.64 * 34.65	34.63 * 34.63	34.71 * 34.71
PML(4, L, 1.0)	29.54 * 29.55	28.78 * 28.84	32.06 * 31.89
PML(4, L, 0.01)	9.458 * 9.207	9.484 * 9.205	9.231 * 9.235
PML(4, P, 0.001)	5.297 * 5.079	5.300 * 5.079	5.333 * 5.082

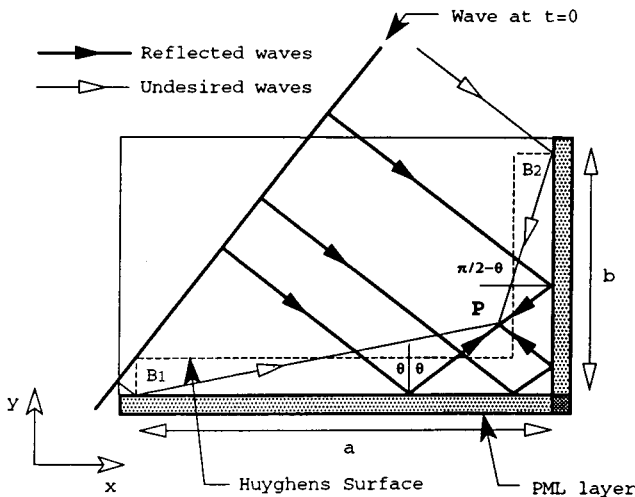


FIG. 8. Computational domain for a plane wave striking a corner.

For different techniques of free-space simulation, Table II compares the field components at P computed by both the FDTD method and the analytical formulas (47). With the first-order one-way technique, the results are in good accordance. Inversely, with the second-order one-way, FDTD results and theoretical values are strongly different. That is not surprising since the second-order discretization cannot be applied at points closest to the corner, where we applied the first-order one. With the operator technique, the second-order discretization can be applied everywhere and the FDTD fields are as expected at both incidences. With the PML technique whose three cases are shown in Table II, the FDTD results can be seen as also in good agreement with the analytical formulas. Moreover, the corner does not add any numerical reflection; the computed results are consistent with those obtained when computing the reflection factor of a wave striking a plane boundary. Indeed, using in (47) the FDTD factors as those of either Table I or Fig. 6 in place of (45) yields values close to those computed with the corner domain. For instance, in the case of the PML(4, L, 1) layer and the 45° incidence, this procedure yields 0.159, 0.159, and 8.141 for the three field components. Such values are very close to the results reported in Table II.

As a conclusion for these experiments, with the PML technique the absorption of outgoing waves at the corners is as good as on the plane boundaries. The corners do not raise any problem nor do they need any special treatment.

### 3.4. Absorption of a Pulse on the Boundaries of a Computational Domain

In order to evaluate the performances of the PML technique when a pulse strikes the boundaries of a computational domain, we have performed the test used in [10] to compare different one-way wave approximations. We have considered the same 100 \* 50 cells domain, with the same space and time increments, respectively, 1.5 cm and 25 ps. The domain was surrounded either by some cells of PML medium or by other boundary conditions. Inversely [10], our computations have been done in the TE case, so the pulse was produced at a magnetic point. With time expressed in nanoseconds, this pulse, set at the point (50, 25) of the mesh, was

$$H_z(50, 25) = \frac{1}{320} (10 - 15 \cos 2\pi t + 6 \cos 4\pi t - \cos 6\pi t) \quad (49.a)$$

$$H_z(50, 25) = 0 \quad \text{if } t > 1 \text{ ns} \quad (49.b)$$

As in [10] a reference solution was computed using a large domain. We used a 400 \* 400 domain, allowing a boundary-free solution during 500 time steps. Denoting  $H_z(i, j)$  the field in the test domain and  $H_{zr}(i, j)$ , its counter-

part in the reference domain, two kinds of results are presented below. First the reflected field along a boundary ( $j=1$ ), at time step 100, normalized to the peak value of the field at point (50, 1),

$$R(i) = [H_z(i, 1) - H_{zr}(i, 1)] / H_{zr}(50, 1)_{\max}, \quad (50)$$

and, second, the  $L^2$  norm of the error on the 100 \* 50 domain, as a function of time,

$$L^2 = \sum_{i=1}^{100} \sum_{j=1}^{50} [H_z(i, j) - H_{zr}(i, j)]^2. \quad (51)$$

Figure 9 shows some results computed when using the one-way and operator techniques, both with second and third orders, and the PML technique in the case of a four-cell linear layer having a 1% normal reflection  $R(0)$ . With this PML layer, the reflected field is about the same as that produced by the third-order techniques. Figure 10 shows the variations of the computed results when reducing the parameter  $R(0)$ , still with a four-cell linear layer. The reflection decreases in the first step, and then increases in the second step when  $R(0)$  goes below 0.01%. Such an evolution is in accordance with that of the reflection factor of a plane wave, as seen on Fig. 6. With the optimum value of  $R(0)$ ,

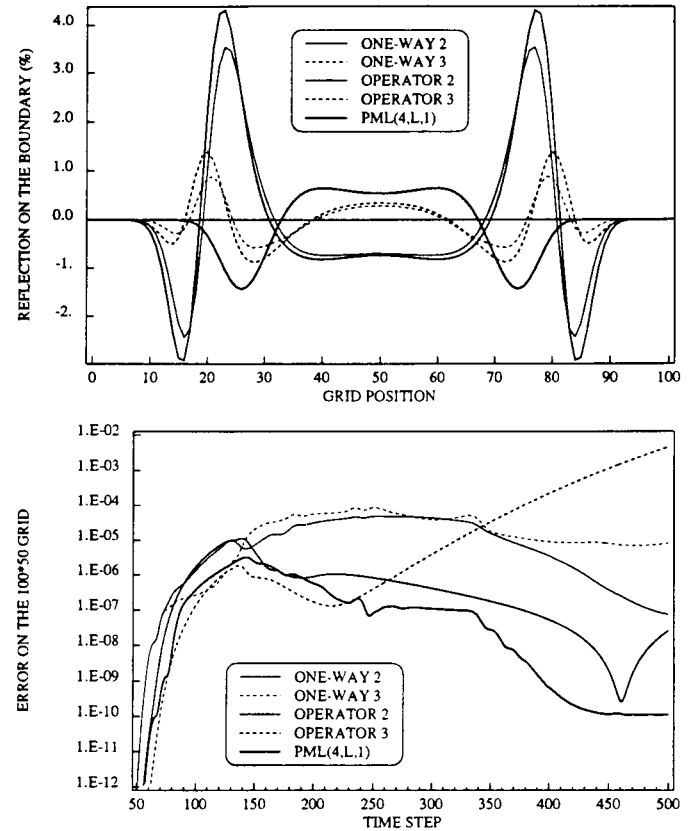


FIG. 9. Absorption of a pulse by one-way, operator, and PML(4, L, 1) techniques.

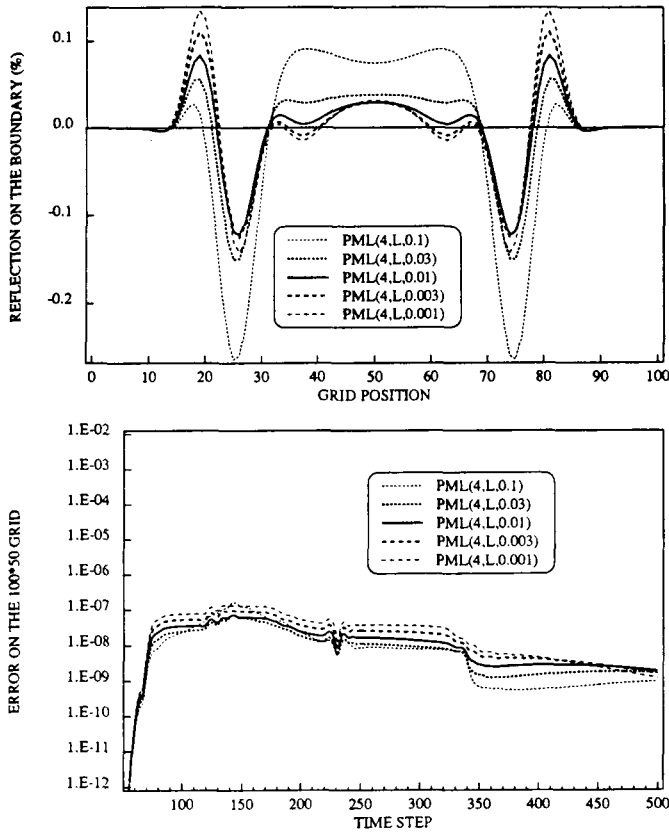


FIG. 10. Absorption of a pulse by a four-cell PML layer for various theoretical factor  $R(0)$ .

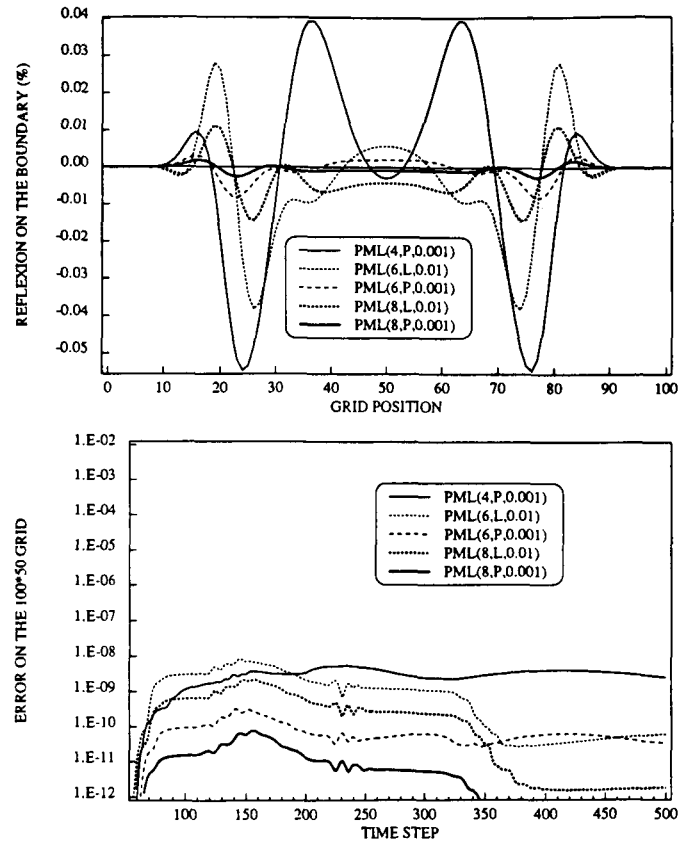


FIG. 11. Absorption of a pulse by four- to eight-cell PML layers.

the reflected field is about 10 times shorter than that of the third-order techniques.

Figure 11 is a comparison of the optimum results obtained with different PML layers, using the procedure of Fig. 10. Layers of four, six, and eight cells are addressed with both linear and parabolic conductivities. As expected, using a parabolic conductivity in place of a linear one reduces the reflection of the pulse. And a greater reduction is obtained when increasing the number of cells. Comparison of Figs. 9 and 11 shows that the PML(8, P, 0.001) layer allows the reflection along the boundary to be about 400 times shorter than that produced by the third-order techniques. Such a factor can be seen also on the average of the magnitude of the reflected field over the entire domain, since the  $L^2$  norm, which is proportional to the energy, is reduced by a factor of the order of 100,000.

In conclusion for these tests, we have observed that the PML technique can drastically reduce the amount of reflection when outgoing waves are striking the boundaries of a computational domain.

### 3.5. Wave-Structure Interaction in the TE Case

Wave-structure interaction problems are the most usual application of the FDTD technique. These open problems

can be satisfactorily solved using the ML or one-way techniques, on condition that the boundaries are set far enough from the scattering structure. In many applications, the structure-boundary distance must be larger than the half-length of the structure. As a result, the greatest part of the computational domain is the vacuum surrounding the scatterer. We will see below that, with the PML technique, the vacuum can be suppressed, and then the computational domain can be widely reduced.

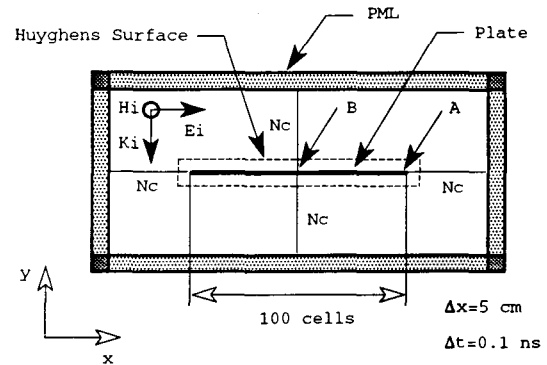


FIG. 12. Computational domain for wave-structure interaction problems.

We have considered the problem of a TE wave scattering on a conducting plate having zero thickness, an infinite width, and a 100 FDTD cells length (5 m). This problem is a two-dimensional one, the principle of computation is presented on Fig. 12. Either the PML layer or another boundary condition is set  $N_c$  cells from the plate and the incident wave is produced by a Huyghens surface one cell from the plate. The results are shown here for a wave of the form:

$$E(t) = E_{inc}[e^{-t/100} - e^{-t}] \quad (\text{time } t \text{ in ns}). \quad (52)$$

In order to test the results, a reference solution was computed in a large domain with  $700 \times 600$  cells surrounded by a 10-cell PML layer. With such a domain, the scatterer-boundary distance was then about three times larger than the scatterer length. The results presented below are, first the normal electric field  $E_y$ , at the end of the plate (A on Fig. 12), and second the magnetic field  $H_z$ , equal to the surface current density, at the middle of the plate (B on Fig. 12).

Figure 13 shows some results computed with various boundary conditions set a half-length from the scatterer.

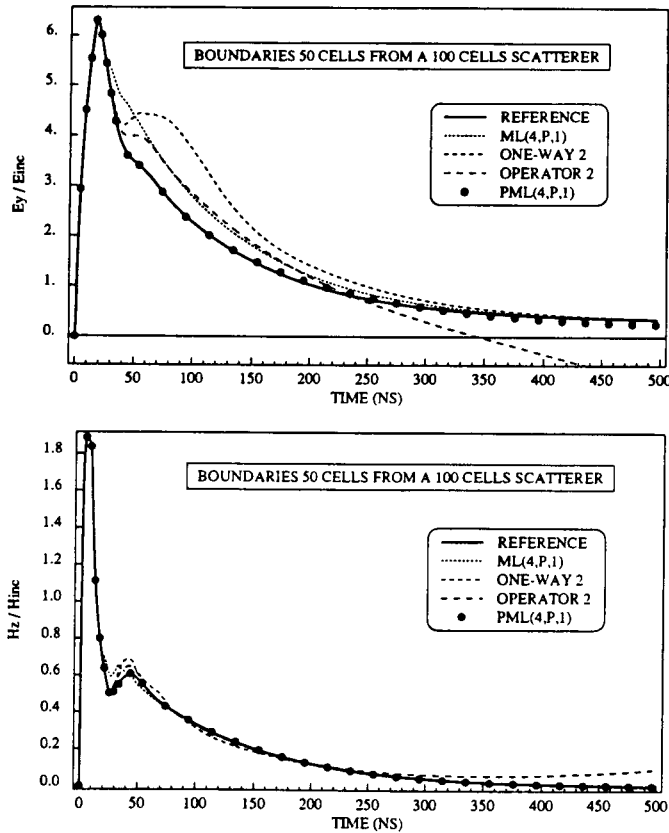


FIG. 13. Wave-structure interaction in the TE case. Electric and magnetic fields computed with boundaries positioned a half-length from the scatterer.

With the four-cell PML used, the results are close to the reference solution. Inversely, with the other techniques they are not satisfactory, a larger domain is needed, the scatterer-boundary distance must be as large as the scatterer length for solving this problem. We note that the best of the other three techniques is the operator (42) at early times, but after 2500 time steps (250 ns) there is a mild instability with this technique.

Figure 14 shows the results computed with PML layers set only two cells from the scatterer and with layer thicknesses varying from 4 to 15 cells. With the four-cell PML layer, the current density could be viewed as close to the reference, but the electric field cannot. Reducing the normal reflection factor  $R(0)$  does not yield better results. Inversely, increasing the number of PML cells yields results that are closer to the reference solution. With 10 cells, the electric field is good, with 15 cells it is perfect. Considering this last case, the solution is computed within a  $134 \times 34 = 4556$ -cell domain, involving about 18,000 field components, while computations with the other techniques of free-space simulation need domains with at least  $300 \times 200$  cells, involving 180,000 field components. For this problem, using the PML technique can then reduce the computer

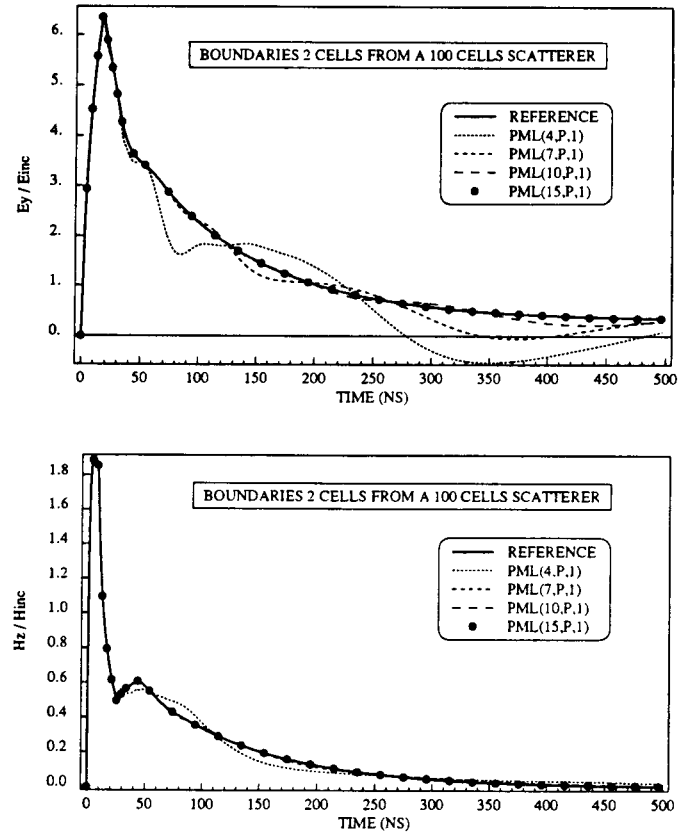


FIG. 14. Wave-structure interaction in the TE case. Electric and magnetic fields computed with the PML layer positioned two cells from the scatterer.

requirements by a factor of 10 for both memory and computational time.

So, the PML technique allows us to solve wave-structure interaction problems without vacuum around the scatterer. The layer must have a thickness of a few cells, but nevertheless the computer requirements can be widely reduced as seen with a two-dimensional problem. Since computers can now accomodate three-dimensional scatterers of 100 cells or more, drastic reductions of such requirements could be hoped for, by extending the PML technique to three-dimensional problems.

### 3.6. Wave-Structure Interaction in the TM Case

We have computed the current induced by a plane wave on a cylinder of a square cross section. This problem was previously solved by the FDTD method in [12] and used in [10] to compare the second and third orders of the one-way technique. Computations have been performed with the same conditions as in [10], with a cylinder of side equal to 20 cells, a 1.592-cm cell, a 100-MHz incident wave propagating normally to one side, and a six-sinusoidal cycles duration. The principle of computation is still that of Fig. 12, except that the square cylinder replaces the thin plate and that Eq. (41) are used in place of (3) in the PML

layer. In order to evaluate the accuracy of the results, a reference solution was computed using a  $1000 \times 1000$  domain which allowed a boundary-free solution during six sinusoidal cycles.

For a domain surrounded by a PML(4, P, 0.01) layer, Fig. 15 presents the magnetic field, equal to the current density, on both the broadside and the shadow side. In each case, the results have been computed with various cylinder-boundary distances, from 2 to 20 cells. We can see that these results are almost perfect for any distance. For 5 to 20 cells, the curves are not distinct from the reference ones, only a slight difference can be observed when the distance equals 2 cells. So, as in the TE case, the PML technique allows us to suppress the surrounding vacuum which is needed when using the ML, one-way, or operator techniques. Then, the computer requirements can be widely reduced too.

### 3.7. Free-Space Radiation of a Slot

We have computed the field radiated by an infinite slot located in a perfectly conducting plane when an electromagnetic wave propagates on one side of that plane. This problem is a two-dimensional one; the principle of computation is shown on Fig. 16. The finite-difference domain is split into two parts by the conducting plane in which a 10-cell wide slot (50 cm) is located. The incident wave above the plane is produced by a Huyghens surface, and the goal of the computation is to obtain the free-space radiated field below the plane.

The computation has been performed within a  $80 \times 42$ -cell domain. The incident plane wave was a Gaussian pulse and the results have been translated to the frequency domain by Fourier transformation. In order to evaluate their accuracy, a reference solution was computed using a  $1000 \times 1000$  domain allowing a boundary-free solution during about 1500 time steps (150 ns), a duration which was also that of the main domain computations.

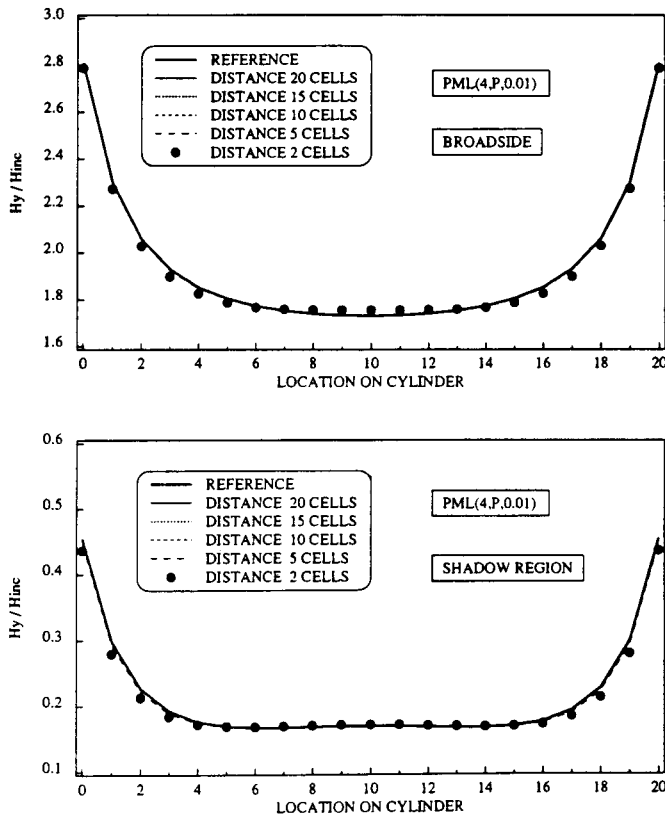


Fig. 15. Wave-structure interaction in the TM case. Magnetic field on a cylinder of square cross section for various cylinder-layer distances.

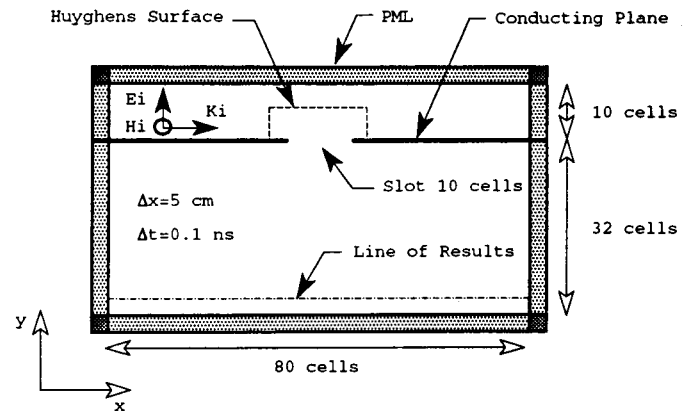


FIG. 16. FDTD domain for computing the radiation of a slot.

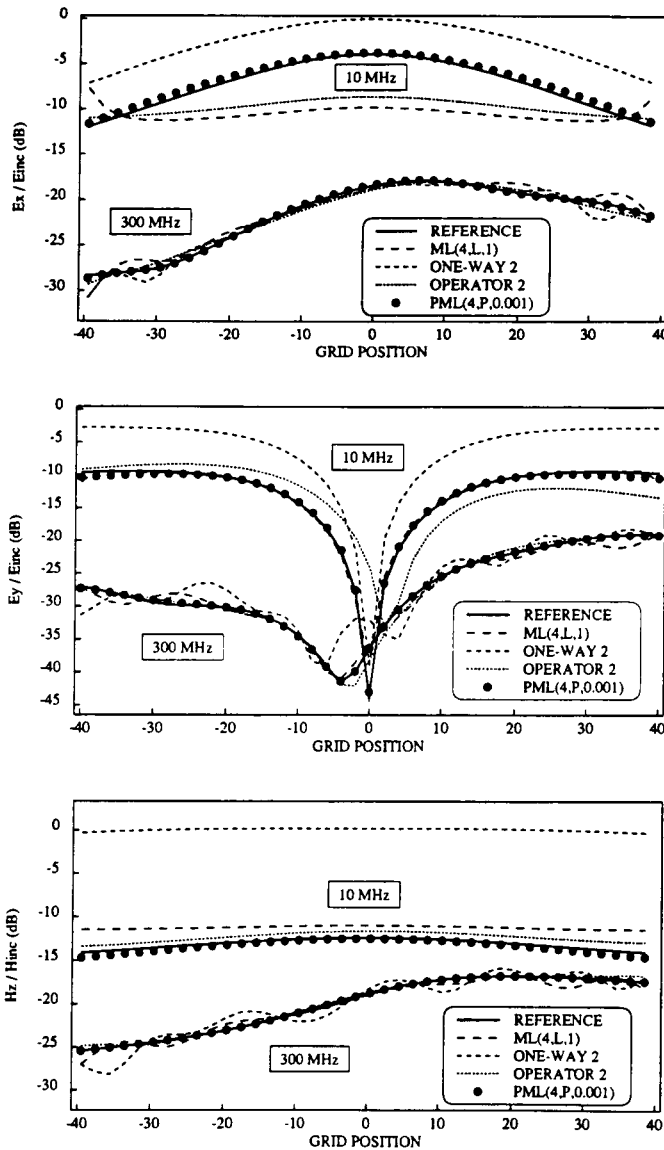


FIG. 17. Radiation of a slot. Components of the field on the line located 30 cells from the slot, computed with ML, one-way 2, operator 2, and PML techniques.

Some results are presented on Fig. 17, along a line located 30 cells below the slot, and then only two cells from the lower boundary conditions. Field components, computed when using either a four-cell PML layer or other boundary conditions, are compared with the reference solution at 10 and 300 MHz. As it appears, the results computed with the PML layer are in good accordance with the reference ones, along the whole line of Fig. 16. That is also

true everywhere in the domain. Inversely, with the other techniques, reflections on boundaries produce errors whose magnitude depends on location, frequency, and component.

#### 4. CONCLUSION

In this paper, an absorbing layer which does not activate any reflection at an interface with first vacuum has been described, and then applied to build a new technique of free-space simulation. This PML technique theoretically allows the electromagnetic waves to be absorbed with a reflection as short as needed. Finite-difference experiments have shown that a small amount of numerical reflection occurs in practical computations, but with a magnitude that can be reduced by tuning some parameters of the layer, especially its thickness. So, one can obtain actual reflection factors that are widely shorter than those of the techniques previously used for free-space simulation. As a result, using the PML technique allows us to obtain a better accuracy in some problems and a release of computational requirements in some others.

After having completed the work related above, two ways of further research were initiated: first, the generalization of the PML technique to three-dimensional problems; second, a more detailed analysis of the wave-structure interaction problem in order to understand how some numerical reflection occurs in the TE case, having in mind a reduction of the layer thickness to be used. The first step has not raised any objection; the second one is still under investigation. These topics will be addressed in further papers.

#### REFERENCES

1. K. S. Yee, *IEEE Trans. Antennas Propag.* **14**, 302 (1966).
2. D. Merewether, *IEEE Trans. Electromagn. Compat.* **13**, 41 (1971).
3. R. Holland, *IEEE Trans. Nucl. Sci.* **24**, 2416 (1977).
4. J. P. Bérenger, Note Technique DGA/ETCA/DET/390, 1977 (unpublished).
5. J. P. Bérenger, in *Actes du Colloque CEM, CNFRS-URSI, Trégastel, France, 1983*.
6. R. Holland and J. W. Williams, *IEEE Trans. Nucl. Sci.* **30**, 4583 (1983).
7. B. Engquist and A. Majda, *Math. Comput.* **31**, 629 (1977).
8. G. Mur, *IEEE Trans. Electromagn. Compat.* **23**, 377 (1981).
9. R. L. Higdon, *Math. Comput.* **49**, 65 (1987).
10. J. Blaschak and G. Kriegsmann, *J. Comput. Phys.* **77**, 109 (1988).
11. A. Taflové, *Wave Motion* **10**, 547 (1988).
12. K. Umashankar and A. Taflové, *IEEE Trans. Electromagn. Compat.* **24**, 397 (1982).